JURNAL REKAYASA PROSES
VOLUME 17, NUMBER 2, 2023, 236–244

RESEARCH ARTICLE

Carbon composite of NiO hydrothermal impregnation from sugarcane bagasse and its electrochemical properties

Al Nadine De Nasti[1], Kyfti Yolanda Siburian[1], Abraham Danofan Sembiring[1], Hans Kristianto[2], Ratna Frida Susanti[2,*], Haryo Satriya Oktaviano[3], Agung Nugroho[1,*]

[1]Department of Chemical Engineering, Faculty of Industrial Technology, Universitas Pertamina, Indonesia
[2]Chemical Engineering Department, Industrial Technology Faculty, Parahyangan Catholic University, Indonesia
[3]Research and Technology Innovation, PT Pertamina (Persero), Indonesia

Received 22 August 2023; revised 26 October 2023; accepted 27 October 2023

OBJECTIVES In this study, we report the synthesis of a NiO-Carbon composite using sugarcane bagasse (SB) waste. SB underwent a two-step calcination process at 400 and 800 °C to produce the pristine carbon sample. Scanning Electron Microscopy (SEM) and adsorption-desorption isotherm analysis indicated the presence of pore structures in the sample. METHODS NiO was added to the pristine carbon samples using the hydrothermal impregnation method at 110 °C, resulting in the formation of the NiO-carbon composite. X-ray diffraction (XRD) pattern and Energy dispersive X-ray spectroscopy (EDX) confirmed the presence of NiO on the carbon structure, with a higher loading of NiO resulting in a greater presence of NiO in the carbon structure. RESULTS The BET surface area increased from 11.85 to 57.81 m^2/g after NiO addition, indicating changes in the pore structure. The electrochemical properties of the pristine carbon sample were compared with those of the NiO-carbon composite samples using a three-electrode system. The specific capacitance of the pristine carbon sample was 89.53 F/g at a current density of 0.05 A/g, while after NiO addition, it increased to 250.53 F/g at the same current density. Calculation of the specific capacitance also revealed that a higher NiO loading had a negative impact on the electrochemical properties, suggesting an optimum NiO loading on the carbon structure. CONCLUSIONS Based on all the results, an optimum NiO loading amount on the carbon structure was identified, impacting the crystallite size, morphology, and electrochemical performance. This work will add to our understanding of converting biomass waste into carbon composite materials that can be used as electrode materials.

KEYWORDS carbon composite; galvanostatic charge-discharge; hydrothermal; nickel oxide; sugarcane bagasse

1. INTRODUCTION

The Industrial Revolution 4.0 created a highly dependent society on electronic technology. The sizeable global energy demand to fuel the world's economy drives sustainable consumption of fossil fuels, leading to a decline in environmental conditions. Therefore, innovating more environmentally friendly energy systems has become a top priority in addressing energy issues and global warming. In this context, supercapacitors showed superiority over traditional energy storage systems such as batteries and fuel cells, with outstanding power density, extraordinary life cycles, fast charging and discharging speeds, and extensive storage capacity (Shao et al. 2018; Wang et al. 2021). Carbon is a sustainable and eco-friendly material, obtainable from various sources, including biomass waste, making it an economical energy storage alternative. It also offers a greener choice than other electrode materials. Despite these benefits, more study is needed to improve the electrochemical performance of carbon materials in supercapacitors. Essential research areas include improving synthesis methods, adjusting pore and surface structures, and exploring new precursors for activated carbon production. Therefore, further study on carbon-based material use for electrode materials is vital for advancing energy storage technology.

There was significant research on transition metal oxides (TMOs) and hydroxides due to their high theoretical capacitance, making them favored pseudocapacitive materials for increased energy density. RuO2 stood out because of its exceptional capacitance, impressive cut-off voltage, and remarkable cyclic stability (Oh and Nazar 2010). However, its high cost limits its practical application utilization. As a result, alternative materials such as NiO (Fan et al. 2012; Ge

*Correspondence: agung.n@universitaspertamina.ac.id; santi@unpar.ac.id

et al. 2012), Co_3O_4 (Li et al. 2011), and MnO_2 (Xu et al. 2007) have been explored. Among these, NiO showed promise as an electrode material due to its high theoretical capacitance (2573 F/g), affordability, environmental friendliness, and physicochemical stability (Karuppaiah et al. 2019). By combining NiO with porous carbon materials, the porous structure of the carbon material can serve as an electron-transport medium, facilitating electron transfer and making the redox reaction of NiO more accessible. Thus, integrating nickel oxide/hydroxide with porous carbon materials is a promising approach for pseudocapacitor applications (Pradiprao Khedulkar et al. 2022). There were several methods to incorporate heteroatom into the carbon structure, such as solution doping (Nugroho et al. 2022b), solid-state (Nugroho et al. 2021), and hydrothermal methods (Askaputra and Yuliansyah 2020; Haraki et al. 2023). The hydrothermal method is preferred due to its simplicity and lower energy requirements than other methods.

Organic residues from various sectors, particularly biomass waste, have recently become an important research focus as a sustainable carbon source for developing suitable porous carbon materials for supercapacitors. This is due to their easy fabrication method, low production cost, abundant availability of raw materials, and eco-friendly. This study uses sugarcane bagasse from a local ice drink vendor as a raw material for carbon composite. Sugarcane bagasse is an abundant and renewable source of biomass, particularly in areas where sugarcane is widely grown. It has a unique structure and high cellulose (33.5%) and hemicellulose content (43.6%), which result in a higher carbon yield upon pyrolysis (Sun et al. 2004). Furthermore, carbon-based materials made from sugarcane bagasse have a relatively high porosity and surface area, making them appropriate for various applications.

Various characterization techniques, including Fourier-transform infrared spectra (FTIR), X-ray diffractometer (XRD), Scanning Electron Microscopy Energy Dispersive X-Ray (SEM-EDX), and nitrogen adsorption-desorption measurements, were employed to analyze the samples and understand their structural and morphological properties. Additionally, electrochemical properties were evaluated using a three-electrode system to assess the practical applications of the synthesized samples. This analysis helps determine the suitability of the materials for energy storage systems. The research presented in this study not only addresses waste management and fossil fuel exploration issues but also contributes to the development of environmentally friendly energy storage solutions. By utilizing agricultural waste like sugarcane bagasse, this research aligns with the principles of the circular economy and offers potential positive impacts on both the environment and the energy sector.

2. RESEARCH METHODOLOGY

2.1 Materials

Materials used in this research were NaOH (CAS-No: 1310-73-2, Merck) as the chemical activator, NiSO4.6H2O (CAS-No: 10101-97-0, Smartlab) employed as the nickel oxide precursor, and Na2SO4 (CAS-No:7757-82-6, Merck) for the electrolyte. Sugarcane bagasse (SB) waste, obtained from a local ice drink vendor, was washed three times using deionized water to remove dirt, followed by drying in an oven at 110°C for 12 hours. The dried SB was ground using a mortar and passed through a 100-mesh sieve until fine SB powder was obtained.

2.2 Synthesis procedures

Synthesis of carbon composite was done via carbonization combined with hydrothermal impregnation process. The schematic of the synthesis process was described in Figure 1.

SB powders underwent a two-step calcination process: precarbonization at 400°C and carbonization at 800°C. In a typical procedure, 5 grams of SB were transferred to a crucible and placed in a muffle furnace at 400°C for two hours. The precarbonized sample (pre-C) was mixed with a 0.1 M NaOH solution (mass ratio 1:4), stirred for 2 hours, and fil-

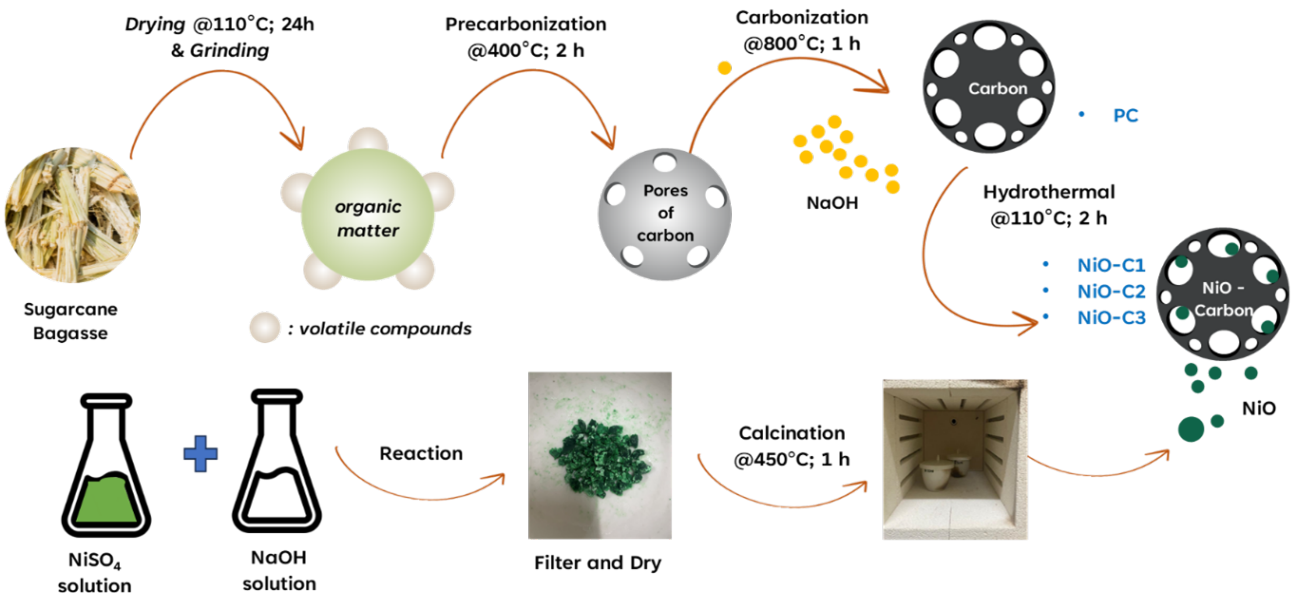

FIGURE 1. Schematic Synthesis of NiO-Carbon composite from Sugarcane Bagasse.

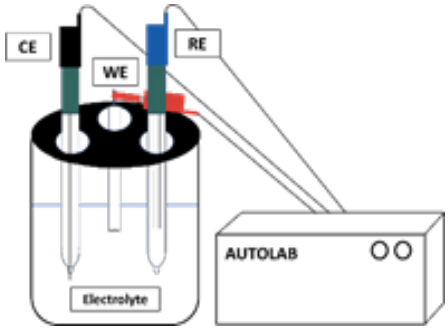

FIGURE 2. Three-Electrode Measurement Layout.

tered using a Whatman Filter paper. The remaining sample was transferred to a crucible and underwent a carbonization process in a tube furnace (MTI OTF-1200X, quartz size of OD 50 x ID 44 x 450 L mm), at a temperature of 800°C for one hour under Ar gas flow. After carbonization, the sample was washed three times with deionized water. The washed sample was then dried in a vacuum oven at 70°C for 8 hours. This sample was designated as PC (pristine carbon sample).

In a separate process, 50 mL of NiSO4.6H2O 1 M was mixed with 50 ml of 2 M NaOH solution and stirred for 30 minutes. Then, the mixture was filtered to produce a green precipitate and dried in an oven at 100°C for 4 hours. The dried solid from the oven was then calcined at 450°C for 1 hour to produce nickel oxide. Impregnation of NiO on the carbon structure was done by the hydrothermal method. The NiO was dispersed in water by mixing 0.1 grams of NiO in 120 ml of deionized water. Pristine carbon samples with amounts of 0.025 gram, 0.05 gram, and 0.1 gram (respectively referred to as NiO-C1; NiO-C2; NiO-C3) were then added to the solution and stirred for 30 minutes. The stirred solution was transferred to a 200 mL Teflon-lined autoclave (dimension of 2.5" x 4.5") and underwent a hydrothermal process at 150°C for 6 hours. After hydrothermal treatment, the sample mixture solution was filtered, washed with deionized water, and dried in a vacuum oven at 70°C for 8 hours.

2.3 Characterization

The crystal structure of the sample was analyzed using an X-ray diffractometer (XRD) ranging between 10°and 80°, using a PANalytical EMPYREAN instrument. Fourier-transform infrared spectra (FTIR) were acquired using a Thermo Scientific iS5 instrument with a 500-4000 cm^{-1} wavelength range. The BET surface area and pore size distribution were determined with a Quantachrome Aswin. The morphology and chemical composition of the elements in the sample were obtained from Scanning Electron Microscopy Energy Dispersive X-Ray (SEM-EDX, Quanta FEG 450), with an accelerated voltage of 20 kV and magnifications of 1000x and 10000x. The electrochemical performance of the synthesized materials was tested with a three-electrode system in an Autolab potentiostat. An Ag/AgCl electrode and Pt wire acted as the reference and counter electrode, respectively, and 1 M Na2SO4 was the electrolyte solution. The working electrode was prepared according to previous research (Haraki et al. 2023; Nugroho et al. 2022a). Cyclic voltammetry (CV) and galvanostatic charge-discharge (GCD) were carried out on an AUT87662 Autolab Potentiostat at room temperature. The system was assembled as displayed in Figure 2.

3. RESULTS AND DISCUSSION

According to the pre-PC yield calculation (Table 1), more than 60% of the mass was lost due to the breakdown of hemicellulose, cellulose, and lignin at high temperatures. Hemicellulose degraded between 220°C and 315°C, with the most rapid breakdown occurring at around 270°C. Cellulose decomposed at temperatures ranging from 315°C to 400°C, with the peak decomposition rate occurring at approximately 350°C. Lignin breakdown occurred over a wide temperature range of 160°C to 900°C (Dwiyaniti et al. 2020). The addition of NiO substantially affected the yield percentage; the more metal added, the higher the yield percentage or remaining mass. Due to its catalytic activity in the CO_2 production reaction, this effect was prevalent in the thermal treatment of carbon employing metal oxide (Nugroho et al. 2021).

Figure 3(a) shows the XRD patterns of all the samples. The XRD results peak at around 21.9°, corresponding to the reflection (002) from the graphite-like carbon structure. Additionally, a peak at 44.3°indicates the plane (101). This structure, known as a turbostratic peak, may consist of a two-dimensional order of layers of carbon planes (Sarkar et al., 2020). In the three samples impregnated with NiO metal, additional peaks are located at 37.3°and 43.2°, with Miller indices (111) and (200), respectively. These peaks indicate the presence of NiO in the carbon structure (Ramos et al. 2021).

Therefore, it can be concluded that NiO has been successfully impregnated into the carbon structure. Meanwhile, the crystallite size of carbon in NiO-C1 (0.87 nm) was the lowest, which may have resulted in the high specific surface area. The crystallite size of the carbon composite sample could negatively correlate with the specific surface area and capacitance. A low crystallite size can also indicate low crystallinity. Metal oxides with low crystallinity or an amorphous structure often yield superior specific capacitance compared to their high-crystalline particles. This phenomenon is primarily due to the increased structural defects and disorder of carbon structure (Owusu et al. 2017).

The functional groups in all the samples were character-

TABLE 1. Calculated Yield Data and Crystallite Size from XRD Pattern.

Sample	Ratio C: NiO	Yield (%)	Crystallite size (nm)
Pre-PC	-	34.8	
PC	-	11.2	21.20
NiO-C1	1 : 0.25	3.4	0.87
NiO-C2	1 : 0.5	3.1	0.95
NiO-C3	1 : 1	2.9	3.99

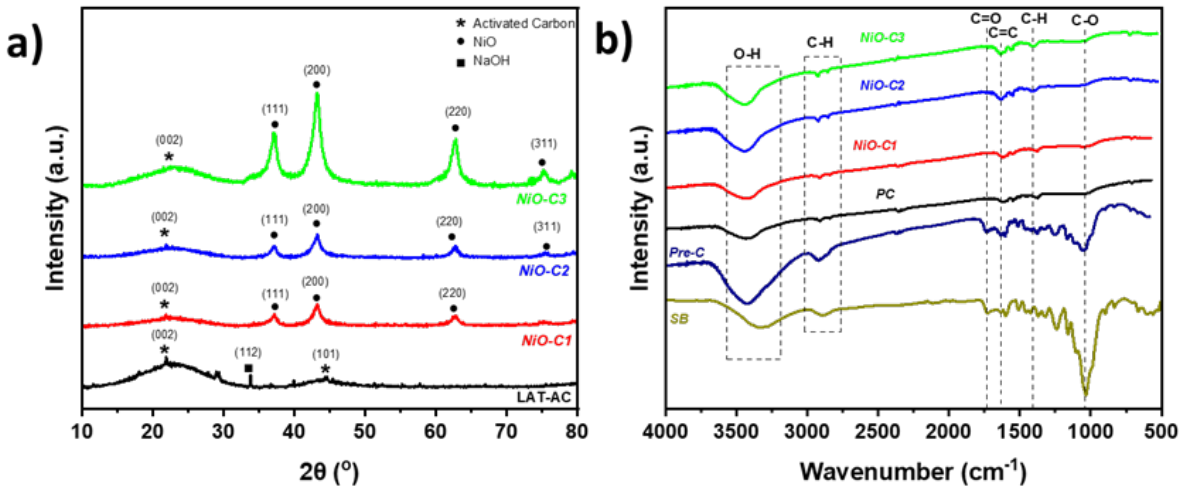

FIGURE 3. (a) XRD pattern and (b) FTIR result of carbon materials after precarbonization, carbonization, and metal oxide impregnation.

ized by FTIR, as shown in Figure 3(b). In the Pre-PC sample (precarbonized only), the spectrum peaks were more prominent, indicating that most of the functional groups in the sample were still clearly detectable. This occurred because the Pre-PC sample was subjected to a low-temperature treatment of 400°C, and its components had not fully decomposed. Subsequently, during the carbonization process at 800°C, the complex organic structure broke down, and volatile components evaporated, causing the spectrum peaks to become flat or nearly imperceptible for the PC and NiO carbon composite. The O-H functional group, found in cellulose and hemicellulose, was also identified in this process. The presence of a fairly dominant O-H functional group is usually associated with O-H bonds in phenol, which are commonly found in carbon materials (Danish et al. 2018). None of the NiO carbon composites exhibited the NiO stretch peak. Several factors could have contributed to this occurrence, such as not all bonds and active functional groups being responsive to IR. More specifically, FTIR detects vibrations between bonds. NiO has a simple and ionic lattice structure, and ionic bonds might not produce strong absorption peaks in FTIR at wavelengths greater than 500 cm^{-1} (Rahdar et al. 2015).

SEM and EDX were used to characterize the morphology of the samples. As depicted in Figure 4, pore structures were observed in all samples after carbonization and NiO impregnation. A previous study also indicated that the SEM image of pre-carbonized SB samples contained few pores (Adinaveen et al. 2013). The pore formation was likely a result of the hydrogen gas generated from NaOH during the carbonization process (Hassan and Youssef 2014). In Figures 4(g) and (h), NiO-C2 and NiO-C3 show a uniform distribution of particles in the pores, corresponding to NiO particles. The EDX results provided further characterization (Figure 4(i-l)), indicating component mapping in the carbon samples. The PC sample only showed C at 98.8% and Na at 1.2%. Due to the numerous and deep cavities of the pores in the pristine carbon, some Na remained trapped within the sample and could not be eas-

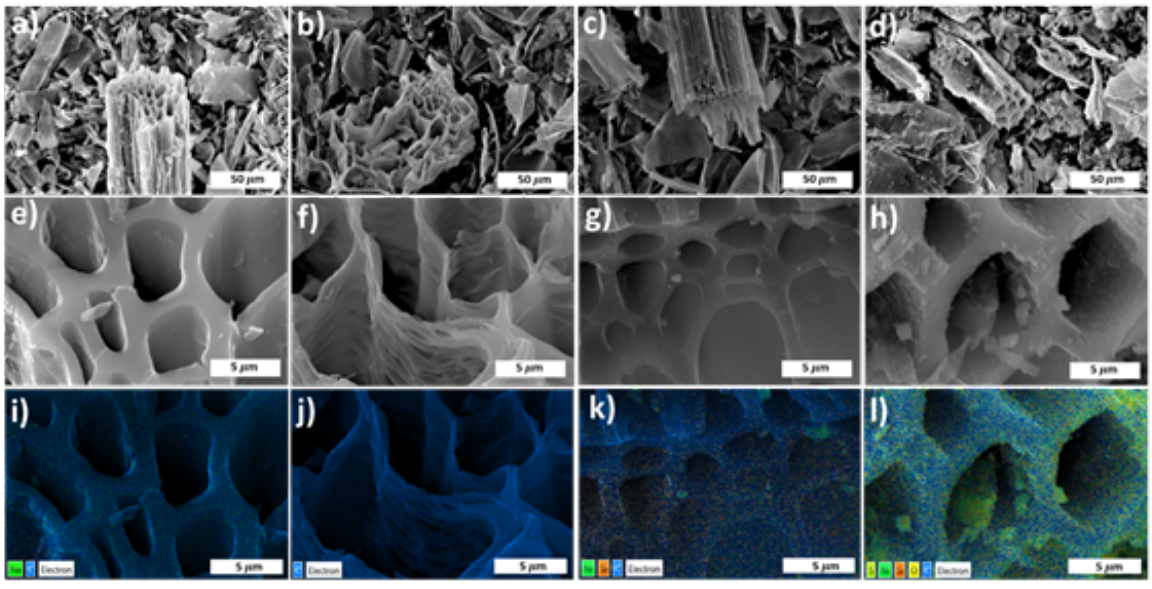

FIGURE 4. (SEM images of (a) PC 1000x, (b) NiO-C1 1000x, (c) NiO-C2 1000x, (d) NiO-C3 1000x, (e) PC 10000x, (f) NiO-C1 10000x, (g) NiO-C2 10000x, and (h) NiO-C3 10000x. EDX images of (i) PC, (j) NiO-C1, (k) NiO-C2, and (l) NiO-C3 impregnation.

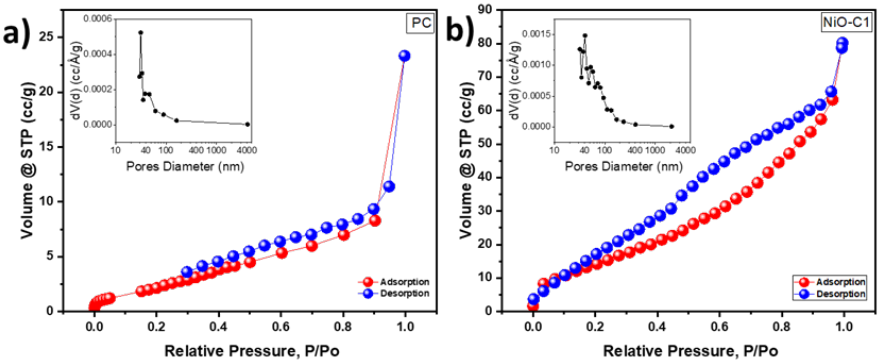

FIGURE 5. (Nitrogen adsorption-desorption isotherm of (a) PC and (b) NiO-C1 1000x. The inset figures shows the pore distribution of the sample.

ily washed out. In the NiO-C3 and NiO-C2 samples (Figure 4(k) and (l)), it was evident that NiO was present, confirming the success of the impregnation process. The green color indicated that the NiO particles were uniformly distributed in the samples. However, some unwanted impurities were still present in the carbon composite, such as Si and S. Si in the EDX spectrum could be attributed to the natural composition of bagasse, which is known to contain silica (SiO_2) (Chindaprasirt and Rattanasak 2020; Khotseng et al. 2022). As for the S, it may have been absorbed from the soil during sugarcane growth and found in various organic forms within plant tissues (Prasad and Shivay 2018).

The specific surface areas of PC and NiO-carbon composites were further determined by nitrogen adsorption-desorption measurements. Figure 5(a) shows that the adsorption-desorption isotherm follows type II of a macroporous structure with a BET surface area of 11.85 m_2/g. The inset of Figure 5(a) also supports the claim that the carbon particles consist of macropores with a diameter of 314.79 nm and a pore volume of 0.03606 cc/g. After the addition of NiO (NiO-C1), the BET surface area increases to 57.81 m^2/g. The isotherm curve (Figure 5(b)) shows hysteresis, indicating an increase in pore volume (0.124 cc/g). The pore size also increases to 404.25 nm. The results of the adsorption-desorption isotherm align well with the morphological structure from the SEM image.

Electrochemical testing was carried out using the CV test for all sample variations. The CV test for PC was conducted in the potential window of -0.3 to 0.7 V, while for PC/NiO, it was performed in the potential window of -0.7 to 0.3 V, with varying scan rates at 5 mV/s, 10 mV/s, 20 mV/s, 50 mV/s, and 100 mV/s. The results of the CV test can be seen in Figure 5. The CV curve for PC closely matched the desired shape, resembling a rectangle. In an ideal state, this rectangular shape indicates that the supercapacitor possesses pure capacitive characteristics, meaning that the charging

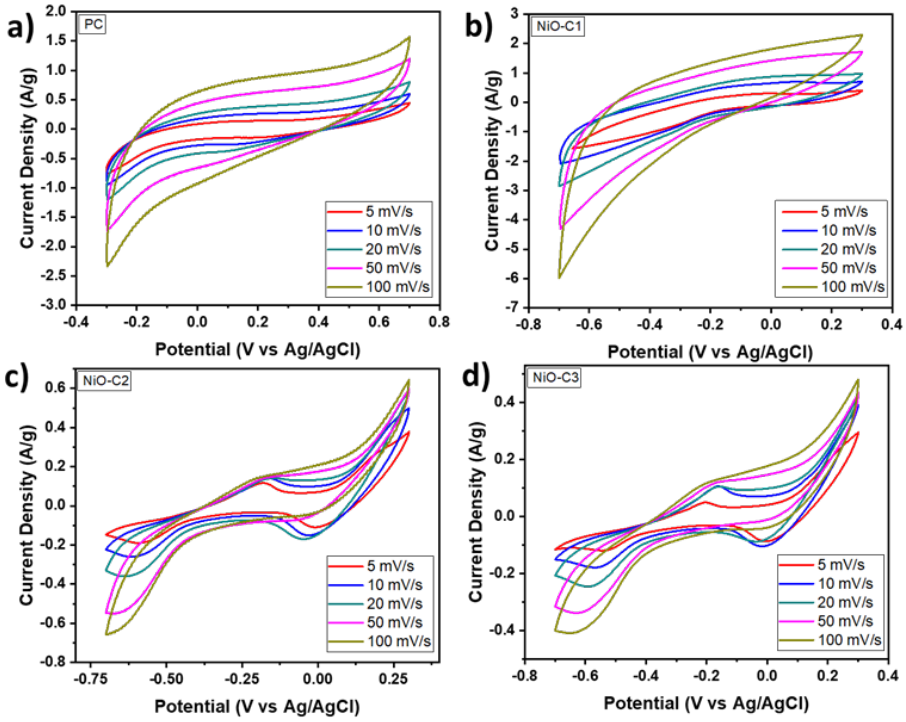

FIGURE 6. CV curves of (a) PC (b) NiO-C1 (c) NiO-C2 (d) NiO-C3 at various scan rate of 5-100 mV/s.

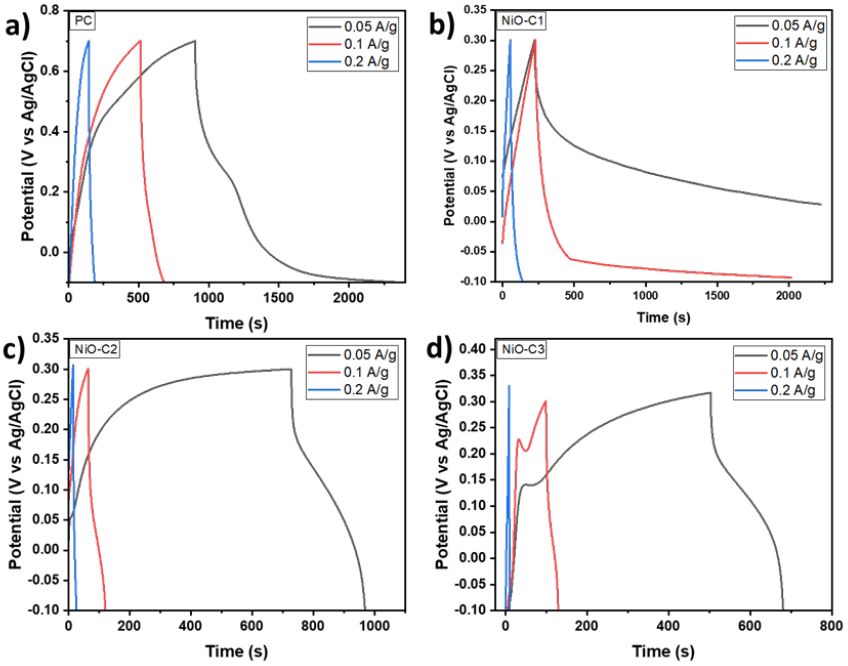

FIGURE 7. GCD curves of (a) PC (b) NiO-C1 (c) NiO-C2 (d) NiO-C3.

and discharging processes occur without any chemical reactions altering the material's form or structure. This rectangular shape should remain consistent during charging and discharging, meaning the CV curve must be symmetrical and show corresponding charging and discharging times. An EDLC (Electric Double-Layer Capacitor) can operate at high charge transfer speeds, as observed from the rectangular shape of the CV curve remaining intact even when the scan rate is increased (Xiong et al. 2021). However, when nickel oxide was added significantly (1:0.5 for NiO-C2; 1:1 for NiO-C3), the shape of the CV curve changed, and a peak appeared. This peak signified the presence of pseudocapacitive behavior, indicating that specific chemical reactions altered the material's structure or form during the charging and discharging processes. This peak appeared at a specific voltage value when the chemical reaction occurred. However, in NiO-C1, the peak indicating pseudocapacitive behavior was not visible. This may have occurred because the proportion of NiO in the sample was possibly too low to show the peak. The pseudocapacitive behavior of NiO might have been overshadowed by the capacitive behavior of carbon, which displayed the typical rectangular CV curve of an EDLC.

If we compare the results of PC with NiO-C1, adding a metal oxide into the composite electrode could help increase capacitance (as observed from the curve area). However, adding an excessive amount of metal oxide could reduce capacitance. Metal oxides tend to have lower electrical conductivity compared to carbon materials. So, if the quantity of metal oxide in the composite was too high, it may have slowed down electron transfer within the electrode, thereby limiting the supercapacitor's power performance. The excessive addition of metal oxide could have also affected the electrode's pore structure and surface area. This might have reduced electrolyte ion access to the electrode surface and decreased

TABLE 2. Specific capacitance of carbon samples.

Sample	Current Density (A/g)	Specific Capacitance (F/g)
PC	0.05	89.53
	0.1	20.93
	0.2	13.50
NiO-C1	0.05	250.53
	0.1	384.57
	0.2	51.39
NiO-C2	0.05	31.00
	0.1	15.99
	0.2	8.65
NiO-C3	0.05	23.02
	0.1	8.98
	0.2	3.48

double-layer capacitance (Zhang and Zhao 2009). All sample variations showed a decreasing curve area as the scan rate increased. The scan rate in CV measurements significantly impacted the specific capacitance value measured. At higher scan rates, electrolyte ions did not penetrate as deeply into the active electrode material's inner surface, as they had less time to permeate into the pores of the electrode material (Javed et al. 2016).

The GCD curves are depicted in Figure 6. The GCD curve for an EDLC should ideally form a perfectly symmetrical triangle that reflects consistent capacitance during the charging and discharging cycles. However, for the pristine carbon sample, the GCD curve shows an asymmetrical triangle. This non-ideality may be due to the relatively high internal resistance of the electrode or the electrochemical cell. This resistance could slow the charging and discharging processes and create curvature in the GCD curve (Andreas and Conway 2006). Another possibility is the presence of impurities or other components in the sample that behave pseudocapacitively. These materials could interact with electrolyte ions and cause redox reactions that affect the GCD curve. Meanwhile, NiO carbon samples show a GCD curve that is a combination of EDLC and pseudocapacitance. This can be observed from the curve's shape, which forms a triangle with curvature, increasing the area of the triangle and resulting in a longer discharge time (Sannasi and Subbian 2020). The presence of curvature indicates the occurrence of redox reactions in the electrochemical system.

The calculation results of the specific capacitance values for all samples are displayed in Table 2. The increase in specific capacitance values after adding NiO is associated with the combined effect of the metal oxide and the carbon-based material.

Nickel oxide, with its high theoretical capacitance, enters the pores of the carbon material, providing more active sites for redox reactions on the material. NiO can react reversibly in the electrochemical process, thereby enhancing the electrochemical performance of the material. Generally, the NiO-C1 material shows the highest specific capacitance results. A ratio of 1:0.25 is the most optimal. Adding more NiO (in ratios of 1:0.5 and 1:1) might disrupt the pore structure or lead to excessive accumulation of NiO, reducing the number of available active sites. Adding NiO in large amounts might disrupt the redox process, for example, by limiting ion diffusion through the material or causing aggregation of NiO particles, which could decrease the capacitance.

The electrode material may not be fully charged because the electrolyte ions need more time to diffuse into the material at a high current density. Therefore, only some active sites participate in the charge-discharge process (Hou et al. 2021). However, different results were obtained in the NiO-C1 sample, where the capacitance at 0.1 A/g is higher than at 0.05 A/g. If the electrode material contains many pores that can be quickly filled and emptied, the capacitance at higher current density might be larger. At a current density of 0.1 A/g, there might be a proper balance between adequate time for ions to diffuse into the pores and a high enough redox reaction rate to provide a significant pseudocapacitive contribution. On the other hand, redox reactions contribute less at a current density of 0.05 A/g, while at 0.2 A/g, the diffusion time is too short to allow ions to reach all active sites within the material.

4. CONCLUSIONS

The transformation of sugarcane bagasse into carbon materials using pre-carbonization and carbonization methods with NaOH has been successful, resulting in the formation of carbon composite structure. XRD analysis confirms the successful addition of nickel oxide (NiO) to the activated carbon. The CV and GCD curves indicate that the impregnated samples exhibit pseudocapacitive properties, suggesting their potential for energy storage applications. The specific capacitance of the pristine carbon sample was 89.53 F/g at a current density of 0.05 A/g, while after NiO addition, it increased to 250.53 F/g at the same current density. At higher current density of 0.1 A/g, the specific capacitance of the NiO-C1 sample, which was impregnated with NiO, was found to be 384.57 F/g. This result indicates an increase in specific capacitance compared to the sample without NiO impregnation. These findings demonstrate the effectiveness of incorporating NiO into the activated carbon for enhancing its energy storage capabilities. This study highlights the promising potential of utilizing agricultural waste, such as sugarcane bagasse, to develop carbon-based materials for energy storage devices. It emphasizes the importance of proper material selection and optimization to achieve improved performance in energy storage applications.

5. ACKNOWLEDGEMENTS

This project is funded by the Directorate Research, Technology and Community Service, Directorate General of Higher Education, Research, and Technology, Ministry of Education, Culture, Research and Technology Republic of Indonesia under the PKDN research scheme 2023. The authors are grateful for the funding.

REFERENCES

Adinaveen T, Kennedy L, Vijaya JJ, Sekaran G. 2013. Studies on structural, morphological, electrical and electrochemical properties of activated carbon prepared from sugarcane bagasse. Journal of Industrial and Engineering Chemistry. 19:1470–1476. doi:10.1016/j.jiec.2013.01.010.

Andreas H, Conway B. 2006. Examination of the double-layer capacitance of an high specific-area C-cloth electrode as titrated from acidic to alkaline pHs. Electrochimica Acta. 51(28):6510–6520. doi:10.1016/j.electacta.2006.04.045.

Askaputra A, Yuliansyah AT. 2020. Pengaruh variasi suhu hidrotermal dan aktivator kalium hidroksida (KOH) terhadap kemampuan hydrochar sebagai adsorben pada proses adsorpsi limbah cair metilen biru. Jurnal Rekayasa Proses; Vol 14, No 2 (2020). doi:10.22146/jrekpros.57394.

Chindaprasirt P, Rattanasak U. 2020. Eco-production of silica from sugarcane bagasse ash for use as a photochromic pigment filler. Scientific Reports. 10(1):9890. doi:10.1038/s41598-020-66885-y.

Danish M, Ahmad T, Hashim R, Said N, Akhtar MN, Mohamad-Saleh J, Sulaiman O. 2018. Comparison of surface properties of wood biomass activated carbons and their applica-

tion against rhodamine B and methylene blue dye. Surfaces and Interfaces. 11:1–13. doi:10.1016/J.SURFIN.2018.02.001.

Dwiyaniti M, Elang Barruna A, Muhamad Naufal R, Subiyanto I, Setiabudy R, Hudaya C. 2020. Extremely high surface area of activated carbon originated from sugarcane bagasse. IOP Conference Series: Materials Science and Engineering. 909(1):012018. doi:10.1088/1757-899X/909/1/012018.

Fan L, Tang L, Gong H, Yao Z, Guo R. 2012. Carbon-nanoparticles encapsulated in hollow nickel oxides for supercapacitor application. Journal of Materials Chemistry. 22(32):16376–16381. doi:10.1039/C2JM32241B.

Ge C, Hou Z, He B, Zeng F, Cao J, Liu Y, Kuang Y. 2012. Three-dimensional flower-like nickel oxide supported on graphene sheets as electrode material for supercapacitors. Journal of Sol-Gel Science and Technology. 63(1):146–152. doi:10.1007/s10971-012-2778-7.

Haraki RE, Arie AA, Susanti RF, Oktaviano HS, Nugroho A. 2023. Synthesis and electrochemical properties of ZnO/activated carbon from vetiver distillation waste. Engineering Chemistry. 2(1):35–41. doi:10.4028/p-1z7h01.

Hassan A, Youssef A. 2014. Preparation and characterization of microporous NaOH-activated carbons from hydrofluoric acid leached rice husk and its application for lead(II) adsorption. Carbon letters. 15(1):57–66. doi:10.5714/CL.2014.15.1.057.

Hou L, Zhou H, Zhai HJ. 2021. Cycling stability depends closely on scan rate: the case of polyaniline supercapacitor electrodes. Soft Materials. 19(4):452–456. doi:10.1080/1539445X.2020.1856872.

Javed MS, Chen J, Chen L, Xi Y, Zhang C, Wan B, Hu C. 2016. Flexible full-solid state supercapacitors based on zinc sulfide spheres growing on carbon textile with superior charge storage. Journal of Materials Chemistry A. 4(2):667–674. doi:10.1039/C5TA08752J.

Karuppaiah M, Sakthivel P, Asaithambi S, Murugan R, Babu GA, Yuvakkumar R, Ravi G. 2019. Solvent dependent morphological modification of micro-nano assembled Mn2O3/NiO composites for high performance supercapacitor applications. Ceramics International. 45(4):4298–4307. doi:https://doi.org/10.1016/j.ceramint.2018.11.104.

Khotseng L, Seroka N, Taziwa R. 2022. Extraction and Synthesis of Silicon nanoparticles (SiNPs) by conventional acid precipitation methods from industrial agro-waste: A mini-review. Applied Sciences. 12(5):2310. doi:10.3390/app12052310.

Li Y, Huang K, Liu S, Yao Z, Zhuang S. 2011. Meso-macroporous Co3O4 electrode prepared by polystyrene spheres and carbowax templates for supercapacitors. Journal of Solid State Electrochemistry. 15(3):587–592. doi:10.1007/s10008-010-1128-3.

Nugroho A, Erviansyah F, Floresyona D, Mahalingam S, Manap A, Afandi N, Lau KS, Chia CH. 2022a. Synthesis and characterization NS-reduced graphene oxide hydrogel and its electrochemical properties. Letters on Materials. 12(2):169–174. doi:10.22226/2410-3535-2022-2-169-174.

Nugroho A, Nursanto EB, Pradanawati SA, Oktaviano HS, Nilasary H, Nursukatmo H. 2021. Fe based catalysts for petroleum coke graphitization for Lithium Ion battery application. Materials Letters. 303:130557. doi:10.1016/j.matlet.2021.130557.

Nugroho A, Wahyudhi A, Oktaviano HS, Yudianti R, Hardiansyah A, Destyorini F, Irmawati Y. 2022b. Effect of iron loading on controlling Fe/N–C electrocatalyst structure for oxygen Reduction reaction. ChemistrySelect. 7(45):e202202042. doi:https://doi.org/10.1002/slct.202202042.

Oh SH, Nazar LF. 2010. Direct synthesis of electroactive mesoporous hydrous crystalline RuO2 templated by a cationic surfactant. Journal of Materials Chemistry. 20(19):3834–3839. doi:10.1039/B926734D.

Owusu KA, Qu L, Li J, Wang Z, Zhao K, Yang C, Hercule KM, Lin C, Shi C, Wei Q, Zhou L, Mai L. 2017. Low-crystalline iron oxide hydroxide nanoparticle anode for high-performance supercapacitors. Nature Communications. 8(1):14264. doi:10.1038/ncomms14264.

Pradiprao Khedulkar A, Dien Dang V, Pandit B, Ai Ngoc Bui T, Linh Tran H, Doong Ra. 2022. Flower-like nickel hydroxide@tea leaf-derived biochar composite for high-performance supercapacitor application. Journal of Colloid and Interface Science. 623:845–855. doi:10.1016/j.jcis.2022.04.178.

Prasad R, Shivay YS. 2018. Sulphur in soil, plant and human nutrition. Proceedings of the National Academy of Sciences, India Section B: Biological Sciences. Volume 88. p. 429–434. doi:10.1007/s40011-016-0769-0.

Rahdar A, Aliahmad M, Azizi Y. 2015. NiO nanoparticles: Synthesis and characterization. Journal of Nanostructures. 5(2):145–151. doi:10.7508/jns.2015.02.009.

Ramos M, Del Angel E, Rojo J, Pacheco Catalán D, Castro M, Mora-Ortiz R. 2021. Activated carbons from coconut shell and NiO-based composites for energy storage systems. Journal of Materials Science: Materials in Electronics. 32:4872–4884. doi:10.1007/s10854-020-05227-0.

Sannasi V, Subbian K. 2020. Influence of Moringa oleifera gum on two polymorphs synthesis of MnO2 and evaluation of the pseudo-capacitance activity. Journal of Materials Science: Materials in Electronics. 31(19):17120–17132. doi:10.1007/s10854-020-04272-z.

Shao Y, El-Kady MF, Sun J, Li Y, Zhang Q, Zhu M, Wang H, Dunn B, Kaner RB. 2018. Design and mechanisms of asymmetric supercapacitors. Chemical Reviews. 118(18):9233–9280. doi:10.1021/acs.chemrev.8b00252.

Sun J, Sun X, Zhao H, Sun R. 2004. Isolation and characterization of cellulose from sugarcane bagasse. Polymer Degradation and Stability. 84(2):331–339. doi:10.1016/j.polymdegradstab.2004.02.008.

Wang G, Lu Z, Li Y, Li L, Ji H, Feteira A, Zhou D, Wang D, Zhang S, Reaney IM. 2021. Electroceramics for high-energy density capacitors: Current status and future perspectives. Chemical Reviews. 121(10):6124–6172. doi:10.1021/acs.chemrev.0c01264.

Xiong S, He Y, Zhang X, Wu B, Chu J, Wang X, Zhang R, Gong M, Li Z, Chen Z. 2021. Hydrothermal synthesis of high specific capacitance electrode material using porous bagasse biomass carbon hosting MnO2 nanospheres. Biomass Conversion and Biorefinery. 11(4):1325–1334. doi:10.1007/s13399-019-00525-y.

Xu MW, Zhao DD, Bao SJ, Li HL. 2007. Mesoporous amorphous MnO2 as electrode material for supercapacitor. Journal

of Solid State Electrochemistry. 11(8):1101–1107. doi:10.1007/s10008-006-0246-4.

Zhang L, Zhao XS. 2009. Carbon-based materials as supercapacitor electrodes. Chemical Society Reviews. 38(9):2520–2531. doi:10.1039/b813846j.